CrossMark

PtNi nanoparticles embedded in porous silica microspheres as highly active catalysts for *p*-nitrophenol hydrogenation to *p*-aminophenol

HUIJUAN GUAN, CONG CHAO, YANJIE LU, HUISHAN SHANG, YAFEI ZHAO, SIGUO YUAN and BING ZHANG*
School of Chemical Engineering, Zhengzhou University, Zhengzhou 450001, P.R. China
e-mail: zhangb@zzu.edu.cn

Abstract. Supported Pt-based alloy nanoparticles have attracted greater attention in catalysis due to their high activity, reduced cost, and easy recycling in chemical reactions. In this work, mesoporous SiO_2 microspheres were employed as support to immobilize PtNi alloy nanocatalysts with different mass ratios of Pt and Ni (1:0, 3:1, 1:1, 1:3 and 0:1) by a facile *in situ* one-step reduction in the absence of any capping agent. SEM, EDS, TEM, FTIR, XRD, ICP-AES, XPS and nitrogen adsorption/desorption analysis were employed to systematically investigate the morphology and structure of the obtained SiO_2 microspheres and SiO_2/PtNi nanocatalysts. Results show that uniform PtNi nanoparticles can be homogeneously and firmly embedded into the surface of SiO_2 microspheres. When the as-prepared SiO_2/PtNi nanocatalysts were used in the reduction process of *p*-nitrophenol to *p*-aminophenol, the nanocatalyst with Pt and Ni mass ratio of 1:3 showed the highest catalytic activity (TOF of 5.35×10^{18} molecules·g^{-1}·s^{-1}) and could transform *p*-nitrophenol to *p*-aminophenol completely within 5 min. The SiO_2/PtNi nanocatalyst can also maintain high catalytic activity in the fourth cycle, implying its excellent stability during catalysis.

Keywords. Porous silica microsphere; Bimetallic alloy; PtNi; nanocatalysts; Hydrogenation reaction.

1. Introduction

p-Aminophenol, an important fine chemical, is widely used in the manufacturing industries, such as pharmaceuticals, dyestuffs, rubber antioxidants and other industrially important products.[1–4] Conventionally, *p*-aminophenol is produced by multi-step iron-acid reduction of *p*-nitrochlorobenzene or *p*-nitrophenol, which causes severe environmental problems by generating a large amount of Fe-FeO sludge.[5,6] To meet the growing demand of *p*-aminophenol, it is important to develop an efficient and green approach for the direct catalytic hydrogenation of *p*-nitrophenol.[7,8] Recently, catalytic hydrogenation of *p*-nitrophenol into *p*-aminophenol by $NaBH_4$ with addition of nanocatalysts has been widely considered as a safe and green process.[9] A large variety of metal nanocatalysts including noble metals, transition metals and their alloys, have been explored for improving the efficiency of this reduction reaction.[10–12] Among them, Pt-based alloys have aroused general concern thanks to their improved catalytic activity for many industrially important reactions, which is attributed to the synergetic effects of Pt and other metals, including geometric effect originated from the lattice contraction and electronic effect caused by the downshift of the d-band center of Pt in the bimetallic structures.[13–18] For example, Ghosh *et al.*, reported that the catalytic activity of PtNi bimetallic nanoparticles is 15 times higher than that of monometallic Pt nanoparticles in the reduction of *p*-nitrophenol.[19] Although bimetallic nanoparticles displayed excellent catalytic properties, their catalytic activities often dropped suddenly after the catalytic transformation because of the aggregation and leaching of the bimetallic catalysts.

Previous studies have revealed that immobilization of bimetallic nanocatalysts onto inorganic or organic supports can improve their stabilization and recycling ability to some extent, such as nanotube or nanofiber, inorganic microsphere and polymer textile and film. Commonly, nanocatalysts are usually attached on the outer surface of the supports due to easy preparation and exposure of active sites.[20–22] However, they may be quickly consumed during repeated use due to weak binding, chemical erosion or excessive stripping. Encapsulation of nanocatalysts with core-shell structure was suggested to be an efficient approach to isolate the inner nanocatalyst core from the external environment, which can protect the inner nanocatalyst and effectively avoid their aggregation and loss during chemical reactions. However, the existence of shell structure on

*For correspondence

nanocatalysts may reduce the diffusivity and heat conductivity of the reaction system, resulting in a decrease in catalytic efficiency.[23−25]

Herein, we prepared porous SiO_2 microspheres consisting of nanoparticles and employed them as support to immobilize PtNi alloy nanocatalysts by a one-step reduction approach which can not only enhance the binding force between nanoparticles and support, but also expose nanocatalysts directly to reactants without sacrificing catalytic activity. The as-prepared SiO_2 microsphere-supported PtNi nanocatalysts show superior catalytic activity (TOF of 5.35×10^{18} molecules·g^{-1}·s^{-1}) toward the reduction of *p*-nitrophenol to *p*-aminophenol, and they can also maintain very high activity in the fourth cycle, implying that the obtained SiO_2/PtNi nanocatalysts possess both high activity and good stability.

2. Experimental

2.1 *Reagents and instruments*

Benzyl alcohol, methylcellulose, octaphenyl polyoxyethylene-10 (OP-10), polyethylene glycol 2000, hydrazine hydrate and $NaBH_4$ were purchased from Tianjin Kemiou chemical reagent Co. Ltd., China; *p*-nitrophenol from Shanghai Macklin biochemical Co. Ltd., China; Absolute ethanol, ethylene glycol, $Ni(NO_3)_2·6H_2O$ and NaOH from Tianjin Fengchuan chemical technology Co. Ltd.; $H_2PtCl_6·6H_2O$ from Sinopharm chemical reagent Co. Ltd. Silica colloidal suspension (GRJ-30) was from Anyang Hongda Jingzhu material Co. Ltd. Double-distilled water was used throughout the experiment. Polyethylene glycol 2000 was chemically pure grade and all other reagents were of analytically pure grade and were used without further purification.

Nitrogen adsorption/desorption isotherms and the corresponding pore size distribution were recorded on Quantachrome NOVA4200 specific surface area and pore size distribution analyzer. Field emission scanning electron microscopy (FE-SEM) images were observed by JEOL JSM-6701F FE-SEM with an energy dispersive X-ray spectroscope (EDS). Transmission electron microscopy (TEM) images were taken using a JEOL JEM-2100 TEM. FTIR spectra were obtained on NICOLET NEXUS-470 FTIR spectrophotometer. X-Ray Powder Diffraction (XRD) data were obtained with a Rigaku Ultima III X-ray diffractometer. The compositions of the catalysts were determined using Shimadzu ICPS-7500 inductively coupled plasma-atomic emission spectrometry (ICP-AES) technique. High-resolution X-ray photoelectron spectroscopy (XPS) was carried out on a VG ESCALAB250 X-ray photoelectron spectrometer. The catalytic activities of the as-prepared catalysts were determined on UV-2450 UV-Vis spectrophotometer.

2.2 *Preparation of mesoporous SiO_2 microspheres*

The synthesis of mesoporous SiO_2 microspheres was carried out by a microemulsion system involving benzyl alcohol, methylcellulose, OP-10, silica colloidal suspension and polyethylene glycol 2000. Benzyl alcohol (20 mL), methylcellulose (1.4 wt%, 1 mL) and OP-10 (19 vt%, 1 mL) were first mixed and stirred at 25°C for 10 min. Then silica colloidal suspension (6 mL) and polyethylene glycol 2000 saturated aqueous solution (6 mL) were added into the above mixture, and uniform surfactant stabilized W/O emulsion was formed with continuous stirring for 30 min. After that, the emulsion was subjected to reduced pressure distillation at 60°C to remove water. The solid was separated by centrifugation followed by washing alternately with water and absolute ethanol, and then dried at 90°C for 24 h. Finally, mesoporous SiO_2 microspheres were obtained by calcination of the sample at 550°C for 2 h.

2.3 *Preparation of SiO_2-supported nanocatalysts*

SiO_2/PtNi nanocatalysts were synthesized by a one-step chemical reduction method in the absence of capping agent. Taking SiO_2/PtNi nanocatalyst with Pt and Ni mass ratio of 3:1 for example, mesoporous SiO_2 microspheres (35 mg) were added to ethylene glycol (80 mL) and ultrasonicated for 1 h to form a stable suspension of SiO_2 microspheres. $H_2PtCl_6·6H_2O$ aqueous solution (0.03352 mol/L, 0.08 mL) and $Ni(NO_3)_2·6H_2O$ (0.9 mg) (with initial mass ratio of Pt:Ni=3:1) were dissolved in ethylene glycol (20 mL). Then, this metal salt solution was added to the above SiO_2 suspension followed by addition of hydrazine hydrate (85 wt%, 0.8 mL) and NaOH ethylene glycol solution (0.375 mol/L, 3.6 mL), and this mixture was kept in an ultrasonic bath for 10 min, and then heated at 110°C for 3 h under N_2 atmosphere. Next, the above suspension was cooled and subsequently separated by centrifugation. The synthesized solid products were thoroughly washed with water and absolute ethanol, and then dried in a vacuum oven at 50°C for 24 h to obtain SiO_2/PtNi (3:1) nanocatalyst with theoretical loading of 2 wt%. For comparison, a series of SiO_2/PtNi nanocatalysts with the same theoretical loading and different mass ratios of Pt and Ni (1:0, 1:1, 1:3 and 0:1) were also prepared using the same method.

2.4 *Catalytic and recycling experiments*

The reduction reaction of *p*-nitrophenol to *p*-amino-phenol was adopted as a probe reaction to quantitatively evaluate the catalytic activity of the as-prepareed catalysts at 25°C, and the process was monitored by UV-Vis absorption spectra. In a typical procedure, freshly prepared *p*-nitrophenol aqueous solution (2×10^{-3} mol/L, 20 mL) and $NaBH_4$ aqueous solution (0.25 mol/L, 20 mL) were mixed to form a uniform solution by stirring for 10 min, and then the prepared catalyst (15.0 mg) were added into the above solution. During the reaction process, 0.5 mL of the reaction solution was taken from the reaction system at a regular interval of 1 min, and subsequently diluted with double-distilled water (9.5 mL). The reaction processes were monitored by measuring the changing of UV-Vis absorbance of *p*-nitrophenol at 400 nm. The sampling procedure was continued until the reaction solution became colorless. The reusability was tested by the same procedure using SiO_2/PtNi(1:3) nanocatalyst.

3. Results and Discussion

3.1 *Characterization of the as-synthesized target products*

The porous structure of the SiO_2 microspheres was characterized by nitrogen adsorption/desorption analysis. SiO_2 microspheres exhibit type-IV adsorption isotherm pattern with a hysteresis loop in the range of P/P_0 0.4-0.9 (Figure 1a). According to the IUPAC classification, the shape of the hysteresis loop is identified as type-H1, corresponding to the cylindrical and narrow mesoporous pores within the SiO_2 microspheres.[26] The SiO_2 microspheres have a specific BET surface area

of 202.63 m²/g and average pore diameter of 3.84 nm (Figure 1b). The large surface area provides ample space for embedding of metal nanoparticles.

The morphology and surface microstructure of SiO_2 microspheres and metal-loaded SiO_2 microspheres were examined by FE-SEM operated at 15 kV in high vacuum. In Figure 2a, it can be seen that spherical SiO_2 with the diameter of about 5–20 μm were obtained. The microspheres are formed by numberous nanoparticles with diameter of 5–15 nm, and the particle stacking endows the microspheres with porous structure (Figure 2b), which is beneficial to the loading of metal particles by embedding them among the nanoparticles. By comparing the surfaces of microspheres and metal-loaded microspheres at low magnification (Figures 2a and 2c), it is found that there are no significant differences on the surfaces, meaning that the metal loading process does not change the overall morphology of SiO_2 support. However, the SEM image of the metal-loaded microspheres at high magnification shows that there are a large number of bright particles on the surface (Figure 2d), which reveals that metal nanoparticles are successfully loaded on the surface of SiO_2 mesoporous microspheres. The loaded metal nanoparticles are uniformly distributed with diameter varying from 20 to 45 nm. A closer examination further reveals that most nanoparticles are embedded into mesoporous microspheres, which can effectively avoid the loss of catalysts and thus improve the catalyst stability (Figure 2d). In addition, the EDS spectrum of metal-loaded SiO_2 microspheres further confirm that the elements of Pt and Ni can be homogenously distributed in the SiO_2 matrix (Figures 2e and 2f).

Figure 3a shows the TEM image of SiO_2-supported PtNi nanocatalysts, the image further confirms the successful loading of metal nanoparticles on mesoporous SiO_2 microspheres. As shown in HRTEM in Figure 3b,
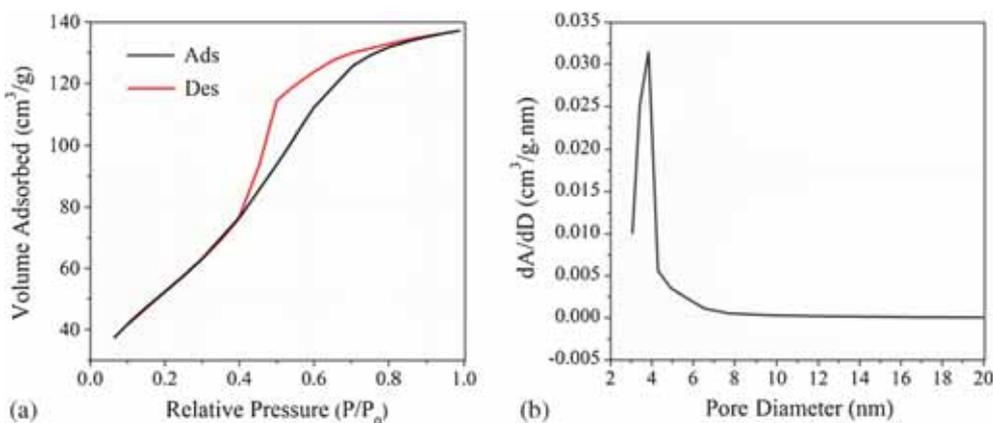

Figure 1. (a) Nitrogen adsorption/desorption isotherms and (b) the corresponding pore size distribution of SiO_2 microspheres.
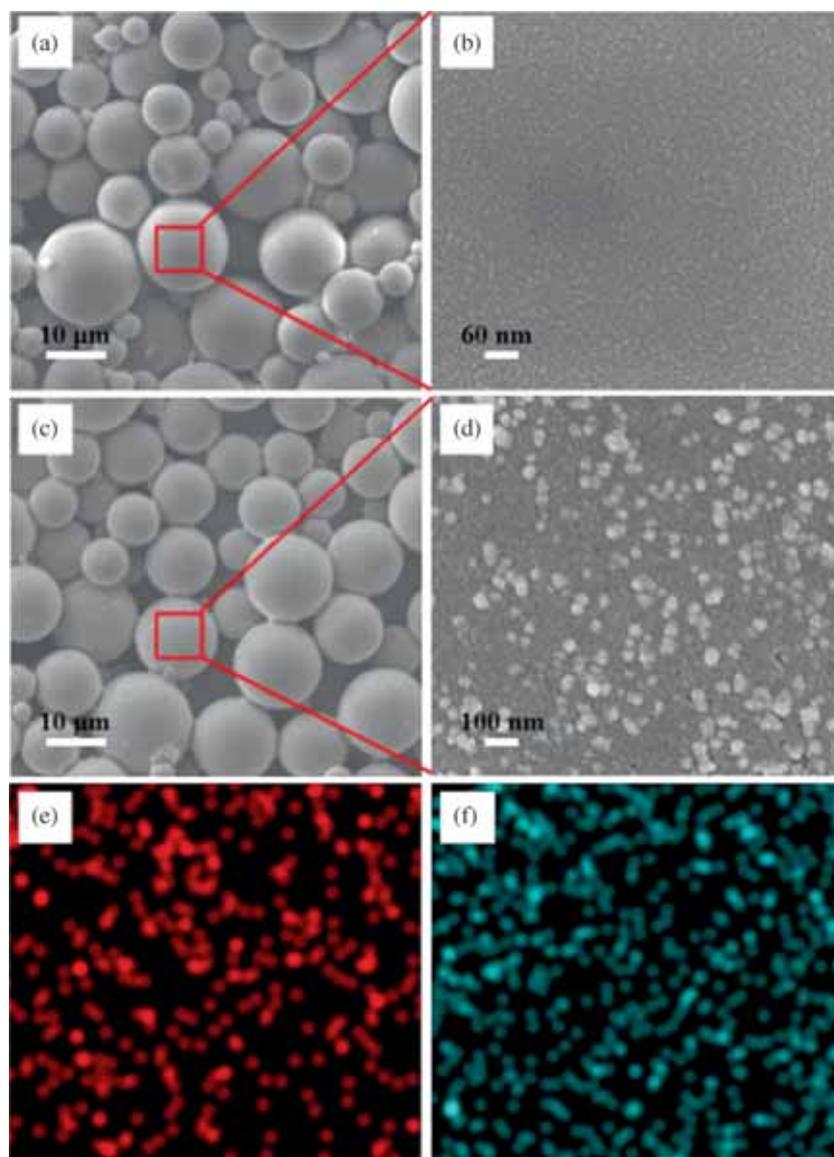
Figure 2. SEM images of SiO$_2$ microspheres: (a) before and (c) after loading metals. The enlarged SEM images of SiO$_2$ microspheres surface: (b) before and (d) after loading metals. EDS elemental mapping images of (e) Pt and (f) Ni distributed in SiO$_2$ microspheres.
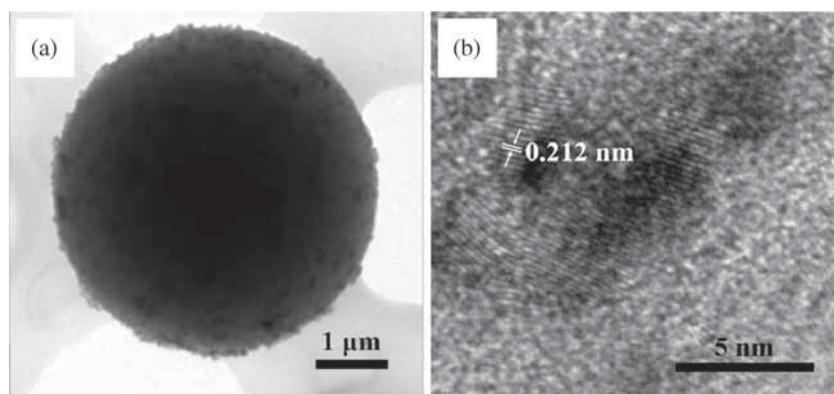

Figure 3. TEM and HRTEM images of SiO$_2$-supported PtNi nanocatalysts.

the lattice spacing of 0.212 nm is smaller than that of the (111) plane of Pt (0.23 nm) and larger than that of pure Ni (0.203 nm), suggesting that PtNi alloy is formed. This result agrees well with the previous report by Sahoo.[27] The lattice fringes correspond to (111) plane of the face-centered cubic (fcc) PtNi alloy.[28]

Figure 4 shows the comparison of the FTIR spectra of SiO_2 and SiO_2-supported nanocatalysts. For the SiO_2 microsphere, the peaks at about 3457 and 1635 cm^{-1} belong to the O-H vibration of SiO_2. The absorption around 1113, 793 and 470 cm^{-1} can be attributed to the asymmetric stretching mode, symmetric stretching mode and bending vibration of Si-O-Si, respectively (Figure 4a). SiO_2-supported nanocatalysts maintain all the characteristic bands of SiO_2 without obvious new absorption appearing in the FTIR spectra
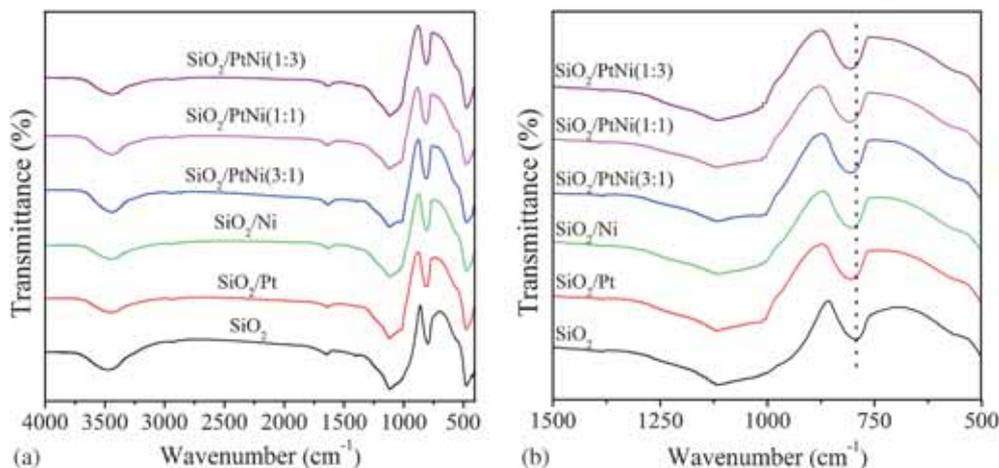

Figure 4. (a) The comparison of the FTIR spectra between SiO_2 and SiO_2-supported nanocatalysts. (b) Partial enlarged FTIR spectra of SiO_2 and SiO_2-supported nanocatalysts.
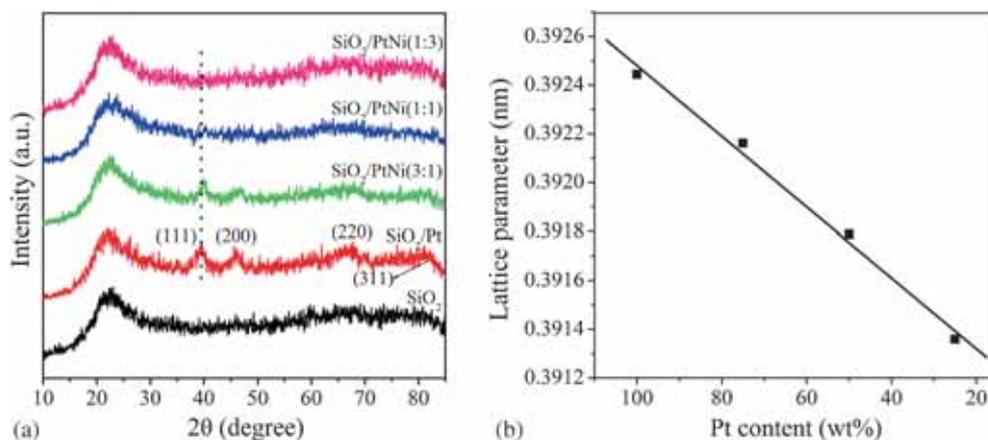

Figure 5. (a) XRD patterns of SiO_2 and SiO_2-supported nanocatalysts. (b) Lattice parameters of Pt in SiO_2/PtNi nanocatalysts with different mass ratios of Pt and Ni (1:0, 3:1, 1:1 and 1:3) deduced from XRD.

Table 1. ICP-AES results of catalysts with different mass ratios.

Catalysts	Pt loading (wt%)	Ni loading (wt%)	Pt+Ni loading (wt%)	Pt/Ni mass ratio
SiO_2/Pt	1.61%	—	1.61%	100 : 0
SiO_2/PtNi (3:1)	1.21%	0.40%	1.61%	75.2 : 24.8
SiO_2/PtNi(1:1)	0.76%	0.81%	1.57%	48.4 : 51.6
SiO_2/PtNi(1:3)	0.39%	1.26%	1.65%	23.6 : 76.4
SiO_2/Ni	—	1.70%	1.70%	0 : 100

(Figure 4a). However, observing from the enlarged FTIR spectra between 1500 cm^{-1} and 500 cm^{-1} in Figure 4b, it is found that the symmetric Si-O-Si stretching modes of the SiO$_2$-supported nanocatalyst are slightly shifted to higher wavenumber values compared with that of pure SiO$_2$, which can be attributed to the loading of metals.[29,30]

Figure 5a shows the XRD patterns of SiO$_2$ and SiO$_2$-supported nanocatalysts. A broad diffraction peak of SiO$_2$ at 2 theta in the range of 20–30° correspond to the amorphous SiO$_2$ (JCPDS 29-0085).[31] For the SiO$_2$/Pt nanocatalyst, there are four diffraction peaks detected at around 39.8, 46.2, 67.5 and 81.3°, which are attributed to the (111), (200), (220) and (311) crystal planes of Pt fcc crystal structure (JCPDS 04-0802), respectively. Diffraction patterns of the SiO$_2$/PtNi nanocatalysts show similar peaks as those of SiO$_2$/Pt nanocatalyst, and the peaks of Pt gradually weakened with the decrease of Pt content. It's worth noting that the Pt (111) diffraction peaks of SiO$_2$/PtNi nanocatalysts are slightly shifted to higher 2 theta values with respect to SiO$_2$/Pt nanocatalyst, and this minor shift in XRD peak position indicates that Ni atoms have gone into the Pt lattice and formed substitution solid solution with Pt.[32] The narrowing of peak (111) of Pt with the increase of Ni content suggests that the lattice parameter of Pt is decreased by occupying the lattice site of Pt with Ni.[33] The lattice parameter of Pt deduced from XRD by software of Jade 6 shows a linear decrease with the decrease of Pt content in SiO$_2$/PtNi nanocatalyst (Figure 5b), which is also indicative of the formation of PtNi alloy.

The actual loading amounts of Pt and Ni in the SiO$_2$-supported nanocatalysts with different mass ratios were analyzed by ICP-AES, and the results are shown in

Table 2. Electronegativities of single metals and calculated effective electronegativities of PtNi bimetals.

Metals	Pt	Ni	PtNi(3:1)	PtNi(1:1)	PtNi(1:3)
$\chi_{effective}$	2.28	1.91	2.09	1.99	1.94

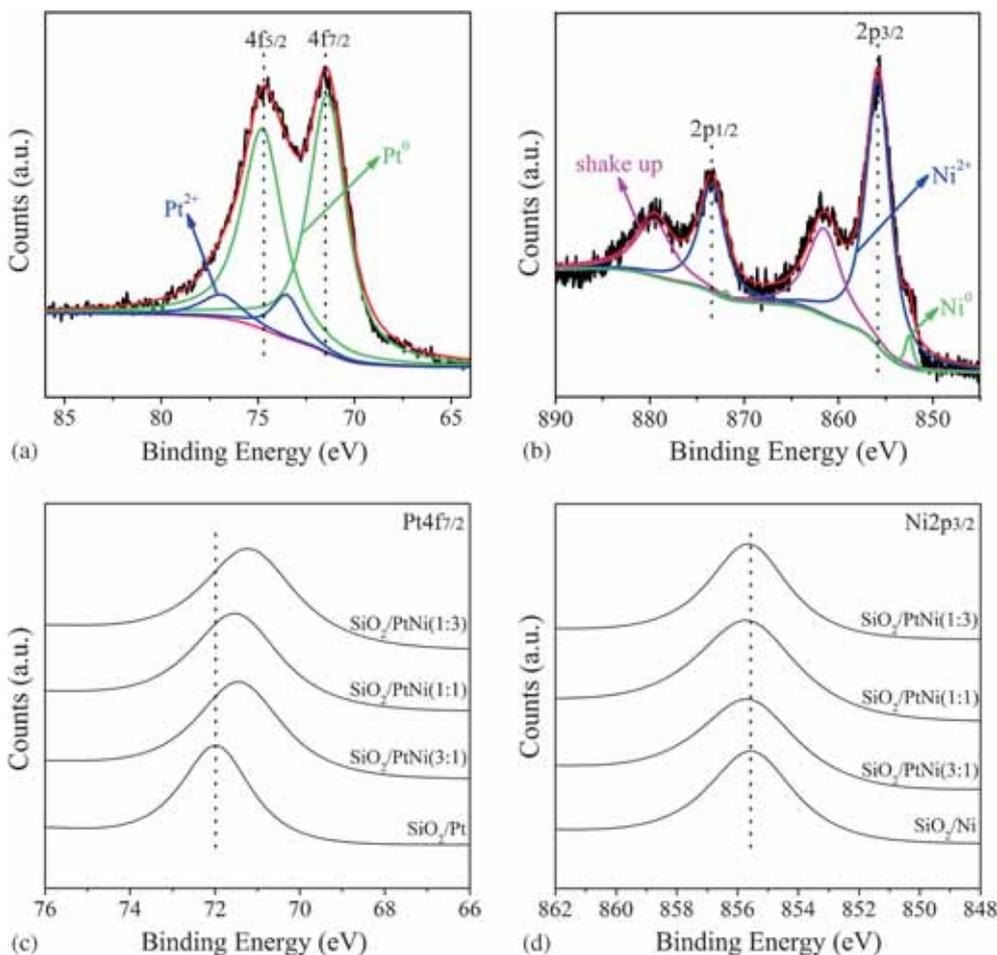**Figure 6.** The XPS spectra of, (a) Pt4f in the SiO$_2$/PtNi(3:1) nanocatalyst; (b) Ni2p in the SiO$_2$/PtNi(1:3) nanocatalyst; (c) The Pt4f$_{7/2}$ peaks of SiO$_2$/Pt and SiO$_2$/PtNi nanocatalysts; (d) The Ni2p$_{3/2}$ peaks of SiO$_2$/Ni and SiO$_2$/PtNi nanocatalysts.
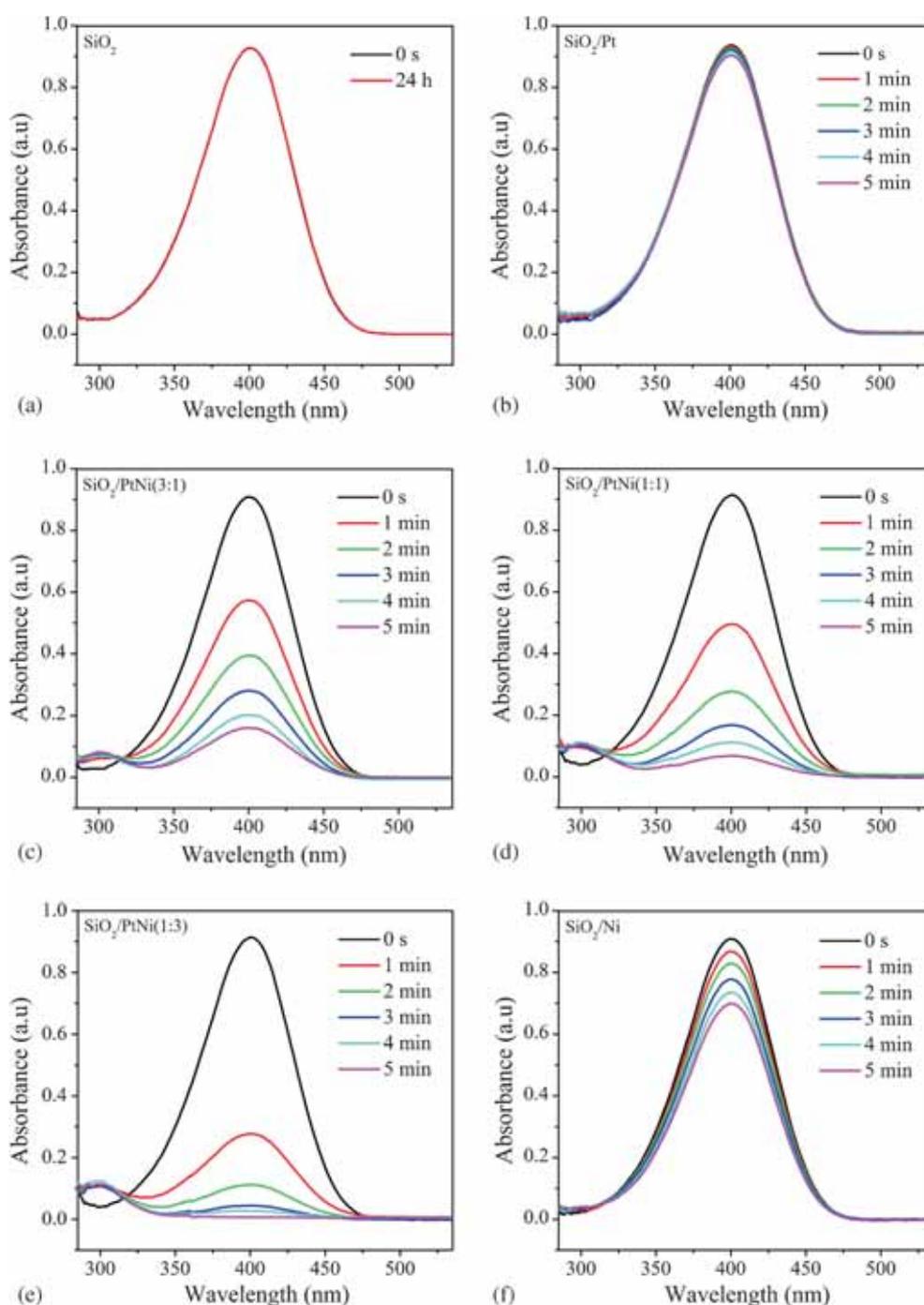
Figure 7. Time-dependent UV-Vis absorption spectral changes of *p*-nitrophenol catalyzed by different catalysts.

Table 1. It is found that the amounts of Pt, Ni and PtNi (Pt+Ni) on the SiO_2 microspheres varied from 1.57% to 1.70% and they are all close to the theoretical loading amount of 2 wt%, implying most of metal ion precursors are reduced to metals and loaded on SiO_2 surface. Besides, the actual mass ratios of Pt and Ni are all approximate to the theoretical mass ratios. Thus, the theoretical mass ratios are adopted in the following description for convenience.

Li *et al.,* proposed a new concept for bi- or multi-metallics, that is, effective electronegativity ($\chi_{\text{effective}}$), and concluded that only alloys whose effective electronegativity is greater than or equal to a critical value (1.93) can indeed be prepared.[34] $\chi_{\text{effective}}$ is determined by the electronegativity of the component metals and the value is given by the following equation:

$$\chi_{effective}(M_x M'_y) = \frac{x}{x+y}\chi_M + \frac{y}{x+y}\chi_{M'} \quad (1)$$

where M and M′ are different metal elements in the alloy, respectively. x and y represent the atom number of M and M′, respectively. χ_M and $\chi_{M'}$ are the electronegativity of M and M′, respectively.

Based on the above formula and ICP-AES results, the $\chi_{effective}$ values of PtNi nanocatalysts were calculated and summarized in Table 2. It can be seen that the $\chi_{effective}$ values of PtNi nanocatalysts are all larger than 1.93, implying the possibility of synthesizing PtNi alloy nanocatalysts with the given composition.

The XPS measurement was used to evaluate the surface structures and chemical states of the SiO$_2$-supported nanocatalysts. Figures 6a and 6b show the XPS spectra of Pt 4f in the SiO$_2$/PtNi (3:1) nanocatalyst and Ni 2p in the SiO$_2$/PtNi(1:3) nanocatalyst, respectively. It can be observed that Pt exists predominantly in Pt form, and the binding energies of Pt 4f ($4f_{7/2} = 71.36$ eV, $4f_{5/2} = 74.76$ eV) are close to the standard values of bulk Pt ($4f_{7/2} = 70.90$ eV, $4f_{5/2} = 74.25$ eV), demonstrating that Pt^{4+} precursor is successfully reduced to form metallic Pt on the SiO$_2$ surface (Figure 6a). In the fine spectra of Ni 2p (Figure 6b), the peaks of 855.64 eV and 873.76 eV are assigned to Ni^{2+} $2p_{3/2}$ and Ni^{2+} $2p_{1/2}$, and the binding energies of 852.52 eV and 871.94 eV are ascribed to Ni $2p_{3/2}$ and Ni $2p_{1/2}$, respectively, suggesting that the dominant surface phases for Ni are oxidized species.[35] Besides, there are two satellite signals at 861.88 eV and 879.63 eV adjacent to the main peaks of Ni, which may be ascribed to multi-electron excitation (shake-up peaks).[36] The Pt $4f_{7/2}$ peaks of SiO$_2$/PtNi nanocatalysts show slight negative shifts compared to that of SiO$_2$/Pt nanocatalyst (Figure 6c), while the Ni $2p_{3/2}$ peaks show positive shifts compared to that of SiO$_2$/Ni nanocatalyst (Figure 6d), which may be caused by the transfer of electrons from Ni to Pt in PtNi alloy.[37,38] In addition, it is also observed that the Pt$4f_{7/2}$ peaks for SiO$_2$/PtNi nanocatalysts are all broader than that of SiO$_2$/Pt nanocatalyst, and the width of Pt$4f_{7/2}$ increases with increasing Ni concentration in PtNi alloy, which may result from the overlap of the Ni3p peak with the Pt$4f_{7/2}$.[39−41]

3.2 *Catalytic properties and reusability of the as-prepared catalysts*

The reduction reaction of *p*-nitrophenol to *p*-aminophenol was adopted as a probe reaction to quantitatively evaluate the catalytic activity of the as-prepared catalysts. The absorbance of *p*-nitrophenol was determined with a UV-Vis spectrophotometer at the maximum wavelength of 400 nm.[42,43] The time-dependent UV-Vis adsorption spectra changes of *p*-nitrophenol catalyzed by different catalysts are compared in Figure 7.

The conversion rates (%) of *p*-nitrophenol to *p*-aminophenol at 5 min for SiO$_2$/Pt, SiO$_2$/Ni, SiO$_2$/PtNi(3:1), SiO$_2$/PtNi(1:1) and SiO$_2$/PtNi(1:3) nanocatalysts are 3.6, 21.5, 82.4, 92.5 and 100.0%, respectively. It is observed that no reduction reaction occurred in the presence of pure SiO$_2$, even after 24 h of experimentation (Figure 7a), indicating that SiO$_2$ microsphere itself cannot be used as catalyst and this reduction reaction cannot proceed without catalyst The result is in good accordance with the previous report by Sahoo.[27] Notably, SiO$_2$/Pt nanocatalyst shows low catalytic activity, the reaction almost did not occur in 5 min (Figure 7b). However, the catalytic activities of SiO$_2$/PtNi nanocatalysts are greatly improved with the increase of Ni content. Among these SiO$_2$/PtNi nanocatalysts SiO$_2$/PtNi(1:3) nanocatalyst showed the highest activity and transformed *p*-nitrophenol to *p*-aminophenol completely within 5 min (Figure 7(c-e)). Furthermore, the absorbance peak of *p*-aminophenol at 300 nm appeared and its intensity increased with reaction time, indicating the conversion of *p*-nitrophenol to *p*-aminophenol.[44] Compared with SiO$_2$/PtNi nanocatalysts, SiO$_2$/Ni nanocatalyst shows a slower catalytic activity (Figure 7f), which reveals that bimetallic nanocatalysts have better catalytic properties than monometallic nanocatalysts. Moreover, the catalytic experiment for the physical mixture of SiO$_2$/Pt and SiO$_2$/Ni (with mass ratio of SiO$_2$/Pt: SiO$_2$/Ni = 1:3) was conducted in order to compare with the catalytic activity of SiO$_2$/PtNi nanocatalysts. The results suggest that SiO$_2$/PtNi nanocatalysts show much higher catalytic activity than that of the physical mixture of SiO$_2$/Pt and SiO$_2$/Ni (Figure S1 in Supplementary Information).

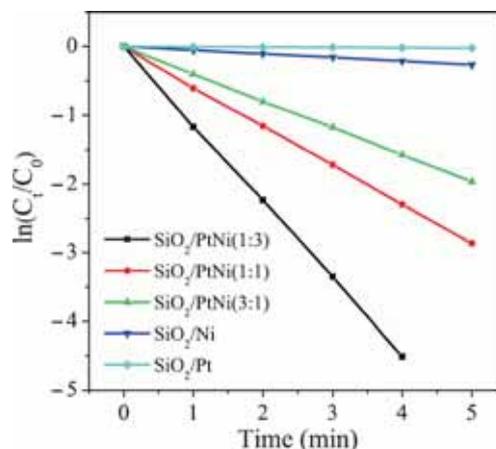The kinetics of this reduction reaction was studied with different catalysts. It usually followed the

Figure 8. Plots of $\ln(C_t/C_0)$ versus time in the presence of different catalysts.

pseudo-first-order kinetics with respect to the concentration of p-nitrophenol,[45,46] as follows:

$$\ln(C_t/C_0) = \ln(A_t/A_0) = -kt \qquad (2)$$

where C_t and C_0 represent the concentrations of p-nitrophenol at times t and $t = 0$, respectively A_t and A_0 are the absorbances of p-nitrophenol (at peak of 400 nm) at times t and t = 0, respectively k is the rate constant.

Figure 8 shows the plots of $\ln(C_t/C_0)$ vs time in the presence of different catalysts. The $\ln(C_t/C_0)$ shows a good linear correlation ($R^2 > 0.999$) with the reaction time for all catalysts, confirming the agreement with pseudo-first-order kinetics. Turnover frequency (TOF) is an important factor for evaluating the efficiency of catalysts In the heterogeneous catalysis, TOF is the

number of reactant molecules that 1 g of catalyst can convert into products in unit time.[47,48] TOF of this reduction reaction can be calculated by using 0.4 mmol of p-nitrophenol and 15 mg of catalysts. The k obtained from the slopes of the linearly fitted plots of $\ln(C_t/C_0)$ vs time and TOF values of different catalysts are given in Table 3. It is obvious that the catalytic activities of the catalysts follow the order of SiO₂/Pt < SiO₂/Ni < SiO₂/PtNi (3:1) < SiO₂/PtNi(1:1) < SiO₂/PtNi(1:3). The catalytic activities of SiO₂/PtNi nanocatalysts are higher than those of SiO₂/Pt and SiO₂/Ni nanocatalysts. The improvement of catalytic activities can be attributed to electronic effect (downshift of the d-band center on PtNi alloy) and geometric effect (the unique structures of PtNi alloys), which can facilitate

Table 3. The k and TOF values for the reduction of p-nitrophenol with different catalysts and the correlation coeffcients for ln (C_t/C_0) vs time plots.

Catalysts	SiO₂/Pt	SiO₂/Ni	SiO₂/PtNi (3:1)	SiO₂/PtNi (1:1)	SiO₂/PtNi (1:3)
k (min⁻¹)	0.0044	0.0525	0.3933	0.5743	1.1214
R^2	0.9999	0.9999	0.9999	0.9998	0.9998
TOF ($\times 10^{18}$) molecules·g⁻¹·s⁻¹	0.19	1.15	4.41	4.95	5.35

Table 4. The comparison of k and TOF of SiO₂/PtNi(1:3) with those of other catalysts reported in the literature for p-nitrophenol hydrogenation to p-aminophenol.

Catalysts	$C_{(p\text{-nitrophenol})}$/mM	k/min⁻¹	TOF($\times 10^{18}$) molecules·g⁻¹·s⁻¹	References
SiO₂/PtNi(1:3)	1.000	1.1214	5.35	This work
RGO/PtNi(25:75)	0.096	0.0672	0.96	[27]
PtNi nanosnowflakes/RGO	0.091	0.1302	—	[9]
Pt-Au ANCs	0.007	0.0800	—	[51]
PtNi(25:75)	0.096	0.0173	0.45	[27]

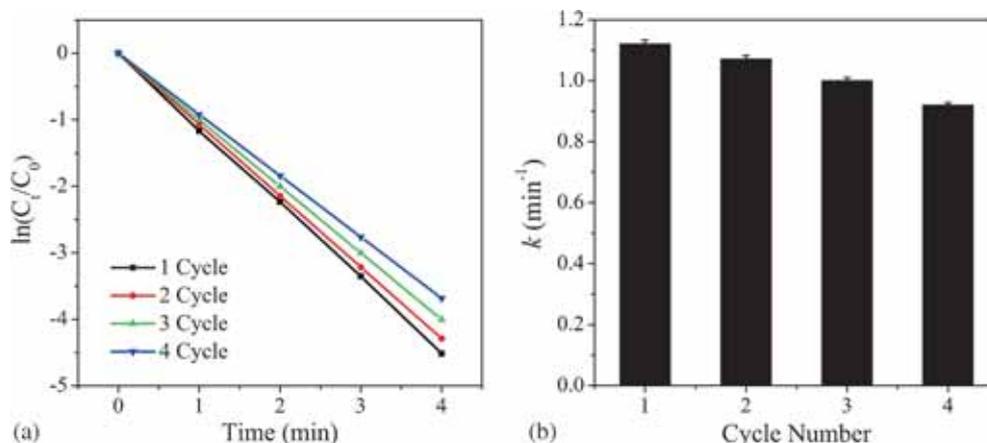$C_{(p\text{-nitrophenol})}$: the initial concentration of p-nitrophenol.

Figure 9. (a) The plots of $\ln(C_t/C_0)$ vs time and (b) the values of k for each cycle with SiO₂/PtNi(1:3) nanocatalyst as catalyst.

the relaying of electrons to *p*-nitrophenol from borohydride ions and endow more activity sites available for the adsorption of reactant molecules.[9,49,50] In addition, PtNi embedded into the surface of mesoporous microspheres, which can expose nanocatalysts directly to the reactants and increase its catalytic efficiency correspondingly.

To further demonstrate the superior catalytic performance of SiO$_2$/PtNi(1:3) nanocatalyst, comparison of *k* and TOF between the as-prepared nanocatalyst and the catalysts reported in the literature are given in Table 4. The *k* of 1.1214 min^{-1} and TOF of 5.35 × 10^{18} molecules·g^{-1}·s^{-1} of SiO$_2$/PtNi(1:3) nanocatalyst for the reduction of *p*-nitrophenol to *p*-aminophenol are much higher than those reported in the literature.[9,27,51] The higher catalytic efficiency may due to the effective loading and uniform dispersion of PtNi nanoparticles on SiO$_2$ support.

Catalytic stability is an important characteristic for practical applications of nanocatalysts.[52,53] In order to evaluate the catalytic stability of SiO$_2$/PtNi nanocatalysts, the representative sample of SiO$_2$/PtNi(1:3) nanocatalyst was tested for reusability in the reduction of *p*-nitrophenol by NaBH$_4$ for several cycles. The plots of ln(C_t/C_0) vs time and the values of *k* for each cycle are shown in Figure 9. It can be seen that the *k* values slightly decrease with the increase in the number of cycles, and the errors are less than 1%. It still can keep 82.08% of the *k* value of original catalyst in the fourth cycle, which is much more stable than that in the previous report where the rate constant for the bare PtNi nanocatalyst drops drastically (about 50%) in the second cycle.[27] These results confirm that embedding PtNi alloy nanoparticles into SiO$_2$ microspheres can improve the catalytic stability of nanocatalysts.

4. Conclusions

In summary, the nanocatalyst PtNi nanoparticles with uniform size can be homogeneously and firmly embedded into the surface of SiO$_2$ microspheres to form SiO$_2$/PtNi nanocatalysts. When the as-prepared nanocatalysts were used in the reduction process of *p*-nitrophenol to *p*-aminophenol, the SiO$_2$/PtNi(1:3) nanocatalyst showed superior catalytic activity (TOF of 5.35 × 10^{18} molecules·g^{-1}·s^{-1}) and could transform *p*-nitrophenol to *p*-aminophenol completely within 5 min. The SiO$_2$/PtNi nanocatalyst can also maintain high catalytic activity in the fourth cycle. The results indicate that the SiO$_2$/PtNi composite can be used as an effective and reusable catalyst for practical applications.

Supplementary Information (SI)

Additional information pertaining to the time-dependent UV-Vis adsorption spectra changes of *p*-nitrophenol catalyzed by physically mixed SiO$_2$/Pt and SiO$_2$/Ni are given in Figure S1, available at www.ias.ac.in/chemsci.

References

1. Du Y, Chen H, Chen R and Xu N 2004 *Appl. Catal. A-Gen.* **277** 259
2. Saha S, Pal A, Kundu S, Basu S and Pal T 2010 *Langmuir* **26** 2885
3. Mandlimath T R and Gopal B 2011 *J. Mol. Catal. A-Chem.* **350** 9
4. Wu K, Wei X, Zhou X, Wu D, Liu X, Ye Y and Wang Q 2011 *J. Phys. Chem. C* **115** 16268
5. Lu H, Yin H, Liu Y, Jiang T and Yu L 2008 *Catal. Commun.* **10** 313
6. Rode C V, Vaidya M J and Chaudhari R V 1999 *Org. Process Res. Dev.* **3** 465
7. Vaidya M J, Kulkarni S M and Chaudhari R V 2003 *Org. Process Res. Dev.* **7** 202
8. Zhang Z, Xiao F, Xi J, Sun T, Xiao S, Wang H, Wang S and Liu Y 2014 *Sci. Rep.* **4** 4053
9. Song P, Feng J, Zhong S, Huang S, Chen J and Wang A 2015 *RSC Adv.* **5** 35551
10. Toshima N and Wang Y 1994 *Langmuir* **10** 4574
11. Lu Z, Yin H, Wang A, Hu J, Xue W, Yin H and Liu S 2015 *J. Ind. Eng. Chem.* **22** 258
12. Hostetler M J, Wingate J E, Zhong C J, Harris J E, Vachet R W, Clark M R, Londono J D, Green S J, Stokes J J, Wignall G D, Glish G L, Porter M D, Evans N D and Murray R W 1998 *Langmuir* **14** 17
13. Ananthan S A, Suresh R, Giribabu K and Narayanan V 2013 *J. Chem. Sci.* **125** 1365
14. Kim J G, Im J K, Ryoo K K, Jeon J Y, Yoo S J and Kim S S 2015 *J. Ind. Eng. Chem.* **22** 258
15. Jeena S E and Selvaraju T 2016 *J. Chem. Sci.* **128** 357
16. Shukla A K, Raman R K, Choudhury N A, Priolkar K R, Sarode P R, Emura S and Kumashiro R 2004 *J. Electroanal. Chem.* **563** 181
17. Ghosh S and Raj C R 2015 *J. Chem. Sci.* **127** 949
18. Stamenkovic V R, Mun B S, Arenz M, Mayrhofer K J J, Lucas C A, Wang G, Ross P N and Markovic N M 2007 *Nature Mater.* **6** 241
19. Ghosh S 2004 *Appl. Catal. A-Gen.* **268** 61
20. Dogan Ü, Kaya M, Cihaner A and Volkan M 2012 *Electrochim. Acta* **85** 220
21. Luo B, Xu S, Yan X and Xue Q 2012 *Electrochem. Commu.* **23** 72
22. Wang M, Shen T, Wang M, Zhang D and Chen J 2013 *Mater. Lett.* **107** 311
23. Seo M, Kim S, Lee D W, Jeong H E and Lee K Y 2016 *Appl. Catal. A Gen.* **511** 87
24. Shet A and Vidya S K 2016 *Sol. Energy* **127** 67

25. Zhang H, Liu J, Tian Z, Ye Y, Cai Y, Liang C and Terabe K 2016 *Carbon* **100** 590
26. Leofanti G, Padovan M, Tozzola G and Venturelli B 1998 *Catal. Today* **41** 207
27. Sahoo P K, Panigrahy B and Bahadur D 2014 *RSC Adv.* **4** 48563
28. Zhu E, Li Y, Chiu C, Huang X, Li M, Zhao Z, Liu Y, Duan X and Huang Y 2016 *Nano Res.* **9** 149
29. Considine D M 1983 In *Van Nostrand's Scientific Encyclopedia* (New York: John Wiley)
30. Williams D H and Fleming I 1987 In *Spectroscopic methods in organic chemistry* (New York: McGraw-Hill)
31. Si Y and Samulski E T 2008 *Chem. Mater.* **20** 6792
32. Yang H, Vogel W, Lamy C and Alonsovante N 2004 *J. Phys. Chem.* **108** 11024
33. Souza L K C D, Zamian J R, Filho G N D R, Soledade L E B, Santos I M G D, Souza A G, Scheller T, Angélica R S and Costa C E F D 2009 *Dyes Pigm.* **81** 187
34. Wang D, Peng Q and Li Y 2010 *Nano. Res.* **3** 574
35. Lan M, Fan G, Wang Y, Yang L and Li F 2014 *J. Mater. Chem. A* **2** 14682
36. Luo B, Xu S, Yan X and Xue Q 2013 *J. Electrochem. Soc.* **160** F262
37. Deng Y, Tian N, Zhou Z, Huang R, Liu Z, Xiao J and Sun S 2012 *Chem. Sci.* **3** 1157
38. Yamauchi Y, Tonegawa A, Komatsu M, Wang H, Wang L, Nemoto Y, Suzuki N and Kuroda K 2012 *J. Am. Chem. Soc.* **134** 5100
39. Haber J A, Cai Y, Jung S, Xiang C, Mitrovic S, Jin J, Bell A T and Gregoire J M 2014 *Energ. Environ. Sci.* **7** 682
40. Haniff M A S M, Lee H W, Bien D C S and Azid I A 2014 *J. Nanopart. Res.* **16** 1
41. Wakisaka M, Mitsui S, Hirose Y, Kawashima K, Uchida H and Watanabe M 2006 *J. Phys. Chem. B* **110** 23489
42. Praharaj S, Nath S, Ghosh S K, Kundu S and Pal T 2004 *Langmuir* **20** 9889
43. Zeng J, Zhang Q, Chen J and Xia Y 2010 *Nano. Lett.* **10** 30
44. Rashid M H, Bhattacharjee R R, Kotal A and Mandal T K 2006 *Langmuir* **22** 7141
45. Lee J, Park J C, Bang J U and Song H 2008 *Chem. Mater.* **20** 5839
46. Lee J, Park J C and Song H 2008 *Adv. Mater.* **20** 1523
47. Saha S, Pal A, Kundu S, Basu S and Pal T 2010 *Langmuir* **26** 2885
48. Saha S, Pal A, Pande S, Sarkar S, Panigrahi S and Pal T 2009 *J. Phys. Chem. C* **113** 7553
49. Raula M, Rashid M H, Lai S, Roy M and Mandal T K 2012 *ACS Appl. Mater. Interfaces* **4** 878
50. Yang J, Shen X, Ji Z, Zhou H, Zhu G and Chen K 2014 *Appl. Surf. Sci.* **316** 575
51. Fu G, Ding L, Chen Y, Lin J, Tang Y and Lu T 2014 *CrystEngComm* **16** 1606
52. Jana D, Dandapat A and De G 2010 *Langmuir* **26** 12177
53. Lin F and Doong R 2011 *J. Phys. Chem. C* **115** 6591